Monte Carlo study of ^{4}He in two dimensions

P. A. Whitlock
Courant Institute of Mathematical Sciences, New York University, 251 Mercer Street, New York, New York 10012

G. V. Chester
Laboratory of Atomic and Solid State Physics, Cornell University, Ithaca, New York, 14853-2501

M. H. Kalos
Courant Institute of Mathematical Sciences, New York University, 251 Mercer Street, New York, New York 10012
(Received 28 December 1987)

The Green's function Monte Carlo and variational methods have been used to calculate the properties of the ground state of two-dimensional liquid and solid ^{4}He described by the HFDHE2 potential. The equation of state, melting freezing transition, radial distribution functions in the liquid and solid, and the momentum distribution in the liquid are all presented. Comparisons are made with three-dimensional ^{4}He and two-dimensional classical systems.

I. INTRODUCTION

Two-dimensional liquid and solid ^{4}He are interesting as idealized models of adsorbed systems and also because they are low-dimensional quantum systems. We have recently initiated a computational program to study these systems. This paper contains our results for the basic properties of the liquid and solid phases. The computation of these properties is a fundamental preliminary before we can start on the more interesting studies of helium films on substrates and on detailed structural studies of the solid phase.

Classical two-dimensional systems have been extensively studied by computer simulations and by experiments.[1] The interest in these systems stems from theoretical work which predicts that the two-dimensional solid will not exhibit long-range crystalline order at finite temperatures.[2,3] Kosterlitz and Thouless[4] introduced the concept of topological defects and used it to predict a novel phase transformation at the melting transition. Clearly it will be of interest to see which, if any, of these ideas apply in a quantum-mechanical two-dimensional solid. We should point out that even the most basic thermodynamic properties of the system may provide evidence about some of the novel features we might expect. For example, does the equation of state predict a strong or weak first-order transition? Does the solid exhibit long-range spatial order? Can the solid be readily formed from the fluid phase? Does the solid exhibit strong metastability or does it readily melt? Underlying these questions is the basic fact that in two dimensions at absolute zero we have no reason to believe that long-range spatial order will be destroyed by long-wavelength phonon fluctuations. We shall see that we are able to provide an answer to the first of these questions. However, the remaining questions can only be answered through the use of better variational and importance functions.

Early computations on two-dimensional ^{4}He involved Hartree calculations.[5,6], integral equation calculations,[7] molecular dynamics,[8] and some Monte Carlo calculations.[9] The first extensive variational Monte Carlo investigation of two-dimensional ^{4}He interacting by the Lennard-Jones (LJ) potential at $T=0$ was reported by Liu, Kalos, and Chester.[10] More recently Ni and Bruch[11] extended the earlier work to other de Boer parameters for the LJ potential and found some change in the melting parameters.

In this paper we present the results of both variational and exact Green's function Monte Carlo (GFMC) calculations. In both types of simulations we used a two-body potential, dubbed HFDHE2, developed by Aziz *et al.*[12] We have computed the equations of state of both the liquid and the solid phases and describe them in Sec. III. A Maxwell double tangent construction yields the melting and freezing densities. Other properties of the two-dimensional system such as the radial distribution function, the structure factor, the condensate fraction in the liquid, and the Lindemann's ratio in the solid are discussed in Sec. IV. In Sec. V, the quantum two-dimensional system, the three-dimensional ^{4}He, and two-dimensional classical systems are compared.

II. METHODS OF ANALYSIS

The Hamiltonian for the system is written as

$$H=-\frac{h^2}{2m}\sum_i \nabla_i^2+\sum_{i<j} V(\,|\,\mathbf{r}_i-\mathbf{r}_j\,|\,)\,, \tag{1}$$

where ∇_i^2 and $\mathbf{r}_i$ are the two-dimensional Laplacian and the position vector, respectively. In variational calculations, we calculate the expectation value of the Hamiltonian, which is an upper bound to the ground-state energy E_0,

$$E_0 \le \frac{\int \psi_T(R)H\psi_T(R)dR}{\int \psi_T(R)\psi_T(R)dR} = \int \frac{H\psi_T(R)}{\psi_T(R)}\frac{\psi_T(R)\psi_T(R)}{\int \psi_T(R')\psi_T(R')dR'}dR\,. \tag{2}$$

The second form of the integral is easily calculated using the method of Metropolis *et al.*[13] and will often give a low variance answer since $H\psi_T(R)/\psi_T(R)$ will be nearly constant if $\psi_T(R)$ is close to the true ground-state wave function. A good trial wave function will be the one that minimizes Eq. (2) with respect to parameters of $\psi_T(R)$. The minimum energy is the best estimate of E_0 for that class of trial function.

The two-dimensional, many-body system was also simulated using the Green's function Monte Carlo (GFMC) algorithm. The details of this method have been described extensively elsewhere[14–16] and will not be discussed here. What we shall discuss is the method by which expectation values are obtained from the GFMC simulations.

The variance of the GFMC calculation is controlled by incorporating importance sampling into the algorithm. A trial wave function is used to guide the random walks into areas of configuration space where the eigenfunction is greatest. Good trial wave functions may be obtained from variational calculations. The output from both variational and GFMC calculations are configurations, which are lists of particle coordinates. The importance sampled GFMC simulation yields sets of configurations chosen from the asymptotic distribution $\psi_T\psi_0$. A "mixed expectation" is defined for any operator F by

$$\langle F\rangle_M=\frac{\int\psi_0(R)F\psi_T(R)dR}{\int\psi_0(R)\psi_T(R)dR}\ . \tag{3}$$

However, we want ground-state expectation values taken with respect to ψ_0. If ψ_0 is an eigenfunction of F, then the mixed expectation is exact, e.g., the total energy calculated with (3) asymptotically approaches E_0. For other operators, further corrections are needed. If we assume that the trial function ψ_T is close to the ground-state wave function, $\psi_T=\psi_0+\delta\psi$, then a linear extrapolation is made to obtain $\langle F\rangle_{\rm ex}$,

$$\langle F\rangle_{\rm ex}=2\langle F\rangle_M-\langle F\rangle_T\ . \tag{4}$$

where $\langle F\rangle_T$ is the expectation value obtained from the variational calculation. The extrapolated expectation value gives $\langle F\rangle_0$ to order δ^2. Other methods[14] exist for obtaining $\langle F\rangle_0$, but have higher variance if δ is small.

The GFMC calculations in three dimensions gave excellent results for liquid and solid ^{4}He.[17] The codes used in the three-dimensional calculations were modified to treat two-dimensional systems and extensively tested. The variational code was tested by performing calculations on ^{4}He with the LJ potential and comparing with the results of Liu *et al.*[10] The GFMC code was tested on a model two-dimensional system for which an exact answer for the energy eigenvalue is known.

The trial function used for liquids in the present calculations has the "Jastrow" form

$$\psi_T(R)=\exp\left[\frac{1}{2}\left[-\sum_{\substack{i,j\\ i<j}}u_2(r_{ij})\right]\right]\ , \tag{5}$$

where $u_2(r_{ij})=(b/r_{ij})^m$ and b and m are variational parameters. For crystal phases of ^{4}He, the trial function in Eq. (5) is multiplied by a one-body Gaussian,

$$\prod_{k=1}^{N}\exp\left[-\frac{c}{2}(\mathbf{r}_k-\mathbf{S}_k)^2\right]\ ,$$

which localizes the particles near the lattice sites $\mathbf{S}_k$. However, this form of the trial function is neither symmetric nor translationally invariant. It is expected that for some properties of the two-dimensional solid, e.g., the one-body density matrix, the use of a symmetric trial function will be important. Therefore, some preliminary calculations were carried out with a trial function containing a symmetric one-body term,

$$\prod_{k=1}^{N}\sum_{l=1}^{N}\exp\left[-\frac{c}{2}(\mathbf{r}_k-\mathbf{S}_l)^2\right]\ .$$

III. EQUATION OF STATE FOR THE FLUID AND SOLID PHASES

A variational search in parameter space was carried out to minimize the energy with respect to b, m, and c in the trial function in Eq. (5). In the liquid phase, a system with 64 particles and periodic boundary conditions was studied. Size effects were estimated by simulating a system with 100 particles. The energies for both size systems agreed within the statistical errors. For the solid, systems of 80 particles were used in the simulation. The values for the variational parameters are listed in Table I for the liquid and Table II for the triangular solid. The two highest liquid densities in Table I and the two lowest solid densities in Table II are metastable liquids and solids, respectively, in the variational equation of state. Therefore, the nonmonotonic behavior of b at these densities is not unexpected. The optimized wave functions were then used as the importance functions in the GFMC calculations.

The equation of state of the two-dimensional liquid is shown in Fig. 1. The variational results are close to the GFMC results at low density but diverge as the density increases. In Table III, the total energies, potential energies and kinetic energies from the Monte Carlo calculations are given. As in three-dimensional ^{4}He, there is a large cancellation between the kinetic and potential energies, with the total energy being a small fraction of either. The two-dimensional liquid is very weakly bound as com-

TABLE I. Variational parameters for the trial wave function given by Eq. (5) for the two-dimensional liquid ^{4}He.

Density (Å^{-2})	b (Å)	m
0.0321	3.042	5
0.0358	3.067	5
0.0421	3.080	5
0.0536	3.399	4
0.0612	3.425	4
0.0658	3.425	4
0.0719	3.502	4
0.0765	3.451	4

TABLE II. Variational parameters for the trial wave function given by Eq. (5) for the two-dimensional triangular solid ^{4}He.

Density (Å^{-2})	b (Å)	m	c (Å^{-2})
0.0612	2.927	5	0.413
0.0689	2.939	5	0.536
0.0765	2.939	5	0.689
0.0842	2.914	5	0.918
0.0918	2.901	5	1.071
0.0995	2.876	5	1.454

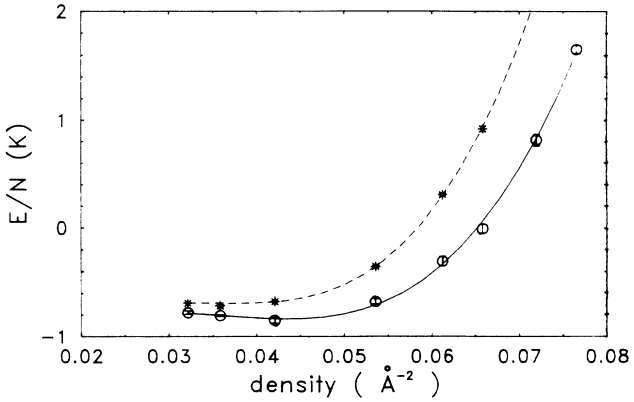

FIG. 1. The equation of state of two-dimensional liquid ^{4}He. The circles with error bars are the GFMC results and the solid line is a fit to those results. The asterisks are energies derived from a variational calculations and the dashed line is a fit to the latter energies.

pared with three-dimensional ^{4}He. We will discuss this comparison in more detail in Sec. V.

The calculated total energies were fit to a function of the form

$$E=E_0+B\left[\frac{\rho-\rho_0}{\rho_0}\right]^2+C\left[\frac{\rho-\rho_0}{\rho_0}\right]^3, \tag{6}$$

where the parameter ρ_0 is the predicted density for the minimum energy E_0. Table IV contains the parameters fitted to the variational and GFMC results. The minimum energy occurs at a lower density in the variational calculation than in the GFMC calculation. The same effect is seen in three-dimensional ^{4}He.

Figure 2 exhibits the equation of state for the triangular solid. The variational and the GFMC results exhibit similar behavior with the GFMC energies always somewhat lower. The total, potential, and kinetic energies in the solid phase are given in Table V for both the variational and the GFMC calculations. As was mentioned earlier, it is anticipated that a symmetric trial wave function will be important for some properties in the solid. Some preliminary calculations were carried out with a symmetric one-body term in the trial function at a density of 0.0765 Å^{-2}. It was necessary to reoptimize the variational parameters with b changing to 3.195 Å and c becoming 0.459 Å^{-2}. The variational energy calculated was much higher, 3.59±0.05 K, as compared with 1.67±0.02 K for the localized trial function. The GFMC calculation converged to an energy of 1.65±0.05 K with the symmetric trial function which is 0.35 K above the energy with the original trial function. This value is identical to the energy of the metastable liquid, 1.65±0.04, at the same density. Subsequent analysis showed substantial diffusion of the particles from the lattice sites and the radial distribution function with the symmetric trial function was identical within statistics to that of the metastable liquid. Vitiello, Runge, and Kalos[18] have recently proposed a new, symmetric, translationally invariant wave function which provides a good description of solid, three-dimensional ^{4}He. We plan to use this type of wave function in the near future to improve our results on two-dimensional solid ^{4}He.

The equation of state of the solid was fit to a cubic polynomial,

$$E=\alpha+\beta\rho+\delta\rho^2+\gamma\rho^3 \tag{7}$$

and the fitted parameters are listed in Table VI. The fitted equations are shown in Fig. 2, as well. The polynomial equations for the liquid and solid were used to locate the freezing and melting densities by a Maxwell double-tangent construction. The results of this calculation are shown in Table VII. Several other determinations of the freezing and melting densities have been carried out from variational calculations using the Lennard-Jones potential. Liu, Kalos, and Chester[10] found that $\rho_l=0.061$ Å^{-2}

TABLE III. Total, kinetic, and potential energies from variational and GFMC calculations in the liquid phase computed using the HFDHE2 potential. All energies are in K/particle.

Density (Å^{-2})	E_v	$\langle V\rangle_v$	$\langle T\rangle_v$	E	$\langle V\rangle$	$\langle T\rangle$
0.0321	−0.69±0.01	−3.26±0.02	2.57±0.02	−0.78±0.02	−3.29±0.07	2.52±0.07
0.0358	−0.71±0.01	−3.80±0.03	3.09±0.08	−0.81±0.01	−3.69±0.05	2.89±0.05
0.0421	−0.67±0.01	−4.75±0.01	4.07±0.02	−0.85±0.03	−4.7±0.1	3.9±0.1
0.0536	−0.35±0.01	−6.30±0.01	5.94±0.02	−0.67±0.03	−6.41±0.04	5.74±0.05
0.0612	0.31±0.02	−7.57±0.01	7.87±0.07	−0.30±0.04	−7.97±0.06	7.68±0.07
0.0658	0.92±0.03	−8.23±0.03	9.15±0.06	−0.01±0.04	−9.03±0.07	9.03±0.08
0.0719	2.13±0.02	−9.58±0.04	11.71±0.07	0.82±0.05	−10.2±0.1	11.0±0.2
0.0765	3.36±0.03	−9.58±0.06	12.94±0.09	1.65±0.04	−11.51±0.07	13.17±0.08

TABLE IV. The parameters fitted to the equation of state function in Eq. (6) for the variational and GFMC results for two-dimensional liquid ^{4}He.

Parameter	Variational	GFMC
ρ_0 (Å^{-2})	0.03731	0.04356
E_0 (K)	−0.6923	−0.8357
B (K)	0.477	1.659
C (K)	3.026	3.493
χ^2/ν of fit	1.08	1.45

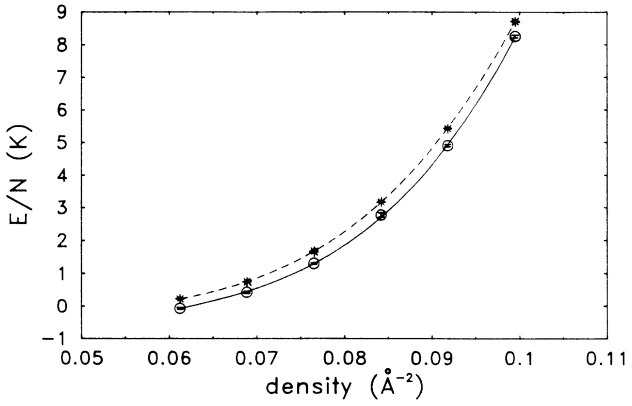

FIG. 2. The equation of state for the two-dimensional, triangular solid ^{4}He. The circles with error bars are the GFMC results with the associated polynomial fit shown by the solid line. Variational energies are indicated by asterisks and the dashed line is a fit to the latter energies.

and $\rho_s=0.070$ Å^{-2}. Further calculations by Ni and Bruch[11] reduced the values to 0.057 and 0.067 Å^{-2}, respectively. Variationally, somewhat similar values are seen with the HFDHE2 potential, $\rho_l=0.0569$ Å^{-2} and $\rho_s=0.0642$ Å^{-2}, as with the LJ results of Ni and Bruch. The GFMC results for the HFDHE2 potential are shifted to higher densities, $\rho_l=0.0678$ Å^{-2} and $\rho_s=0.0721$ Å^{-2}. Similar behavior was observed in three-dimensional ^{4}He (Ref. 17) where the GFMC freezing and melting densities are shifted to higher values (and thereby closer to experiment) compared with the variational results. In that work it was argued that the variational lower bounds are better for the energy of the solid phase than for the liquid phase. Since the configuration space of the solid is simpler than that of the liquid, it is easier to construct good solid trial functions. A glance at Fig. 2 suggests that the analogous argument may also be made for two-dimensional ^{4}He. If there is a basic asymmetry in the variational results which always favors the solid phase, then the variational results will produce transition densities that are too low.

IV. OTHER PROPERTIES

A. The radial distribution function

The radial distribution function was determined for several densities in the liquid and solid phase from the (GFMC) configurations. In Fig. 3, $g(r)$ is shown for two densities in the liquid. The solid line represents the data for $\rho=0.0421$ Å^{-2}, the liquid density nearest equilibrium. The peak value of $g(r)$ is 1.23. This can be compared with the value of 1.38 observed at equilibrium in the three-dimensional ^{4}He system.[17] The dashed line shows the data for $\rho=0.0658$ Å^{-2}, the liquid density nearest the freezing density. At the higher density there is considerably more structure present though no strong indication of the longer-range order seen in the solid. The maximum value of $g(r)$ is 1.54 which is the same as the value observed at the freezing density in three-dimensional ^{4}He.

Figure 4 presents the structure function for the two liquid densities discussed above. The peak of $s(k)$ at the higher liquid density is 1.69 to be compared with 1.59 observed in the three-dimensional system. For a wide range of classical central-force fluids, the first peak in $s(k)$ reaches a value of 2.85 along the freezing line. Thus the two-dimensional quantum liquid more closely resembles the quantum three-dimensional system than a classical liquid.

The radial distribution function at two solid densities is displayed in Fig. 5. At the lower density, $\rho=0.0765$ Å^{-2}, just above the melting density of 0.0719 Å^{-2}, the peak height is 1.67±0.02. In the three-dimensional ^{4}He system, the maximum value of $g(r)$ at the melting density is 1.60±0.02.

TABLE V. Total, kinetic, and potential energies from variational and GFMC calculations in the triangular solid computed using the HFDHE2 potential. All energies are in K/particle.

Density (Å^{-2})	E_v	$\langle V\rangle_v$	$\langle T\rangle_v$	E	$\langle V\rangle$	$\langle T\rangle$
0.0612	0.23±0.02	−7.54±0.04	7.78±0.07	−0.07±0.03	−7.85±0.08	7.79±0.09
0.0689	0.75±0.01	−9.19±0.02	9.94±0.04	0.43±0.03	−9.42±0.08	9.85±0.09
0.0765	1.67±0.02	−11.03±0.06	12.7±0.1	1.30±0.02	−11.07±0.06	12.37±0.06
0.0842	3.18±0.02	−12.62±0.05	15.79±0.07	2.78±0.07	−12.7±0.1	15.5±0.2
0.0918	5.43±0.03	−13.69±0.02	19.05±0.06	4.91±0.03	−14.2±0.2	19.1±0.2
0.0995	8.71±0.02	−14.77±0.05	23.49±0.08	8.26±0.04	−15.1±0.2	23.4±0.2

TABLE VI. The fitted parameters to the equation-of-state function in Eq. (7) for the variational and GFMC results for the triangular solid ^{4}He.

Parameter	Variational	GFMC
α(K)	-13.540	-23.545
β(K Å^2)	671.79	1061.9
δ(K Å^4)	-1.1772×10^4	-1.6875×10^4
γ(K Å^6)	7.3043×10^4	9.4608×10^4
χ^2/ν of fit	0.14	0.48

B. The single-particle distribution

Further insight concerning the solid can be gained from the single-particle distribution function and its moments. In the three-dimensional study of ^{4}He with the Lennard-Jones potential,[19] it was found that the particles exhibited a Gaussian distribution about the lattice sites. The quantity, $\beta=\langle r^4\rangle/2-\langle r^2\rangle^2$, which is identically zero for a two-dimensional Gaussian distribution, is a measure of the departure from the latter. In Table VIII $\langle r^2\rangle$, $\langle r^4\rangle$, and β are given for several densities in the solid. The single-particle distribution function is an accurate Gaussian within our errors at all densities considered. Another quantity of interest is Lindemann's ratio, $L=\langle r^2\rangle^{1/2}/d$, where d is the nearest-neighbor distance. In the three-dimensional Lennard-Jones study mentioned above, the Lindemann's ratio at melting was 0.267. In path-integral Monte Carlo calculations of three-dimensional ^{4}He with the HFDHE2 potential, Runge[20] finds L to be 0.23 at the melting density at $T=4$ K. A linear interpolation of the data in Table VIII, gives a Lindemann ratio of 0.254 at the melting density of 0.0719 Å^{-2}. The Lindemann ratio decreases rapidly with increasing density and by $\rho=0.0995$ Å^{-2} it is 0.182 ± 0.001; thus the particles are tightly localized about their lattice sites. This is also reflected in the structure seen in $g(r)$ at this density in Fig. 5.

C. Condensate fraction and the momentum distribution

Another quantity of interest is the one-body density matrix $n(r)$ whose asymptotic limit n_0 is the fraction of particles condensed into the zero-momentum state. In their variational calculations, Liu, Kalos, and Chester[10] found a value of 0.38 of the condensate fraction at the density $\rho=0.0358$ Å^{-2}. At solidification, $\rho=0.0612$ Å^{-2}, they calculated a value of 0.12 for n_0. In the present calculations, the variational and GFMC results exhibit different density dependence. Near the equilibri-

TABLE VII. The melting-freezing transition for two-dimensional ^{4}He from variational and GFMC calculations.

Method	ρ_l (Å^{-2})	ρ_s (Å^{-2})
Variational	0.0569	0.0642
GFMC	0.0678	0.0721

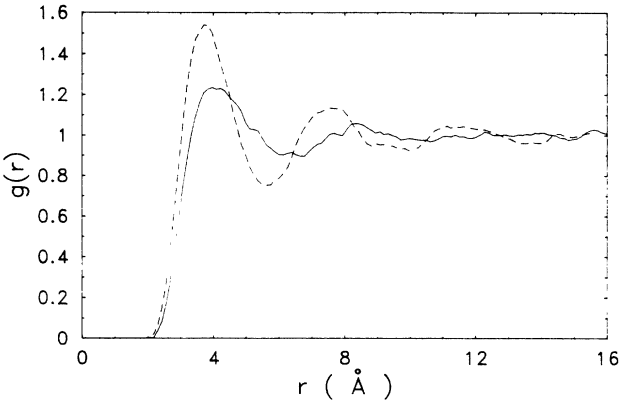

FIG. 3. The radial distribution function at two densities in the liquid. The solid line represents a density near equilibrium, $\rho=0.0421$ Å^{-2}, and the dashed line is a density just before freezing, $\rho=0.0658$ Å^{-2}.

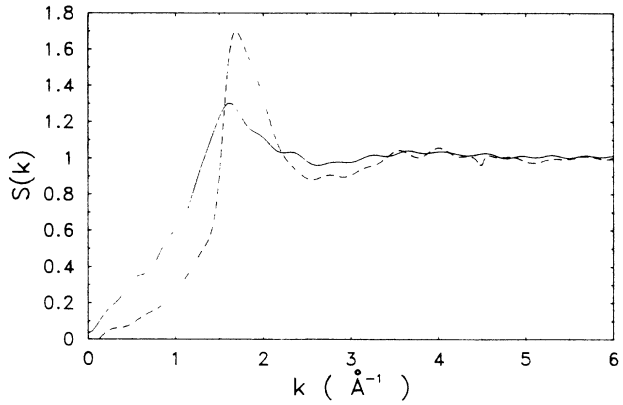

FIG. 4. The structure function for two densities in the liquid. The solid line is a density near equilibrium, $\rho=0.0421$ Å^{-2}, and the dashed line displays a density just before freezing, $\rho=0.0658$ Å^{-2}.

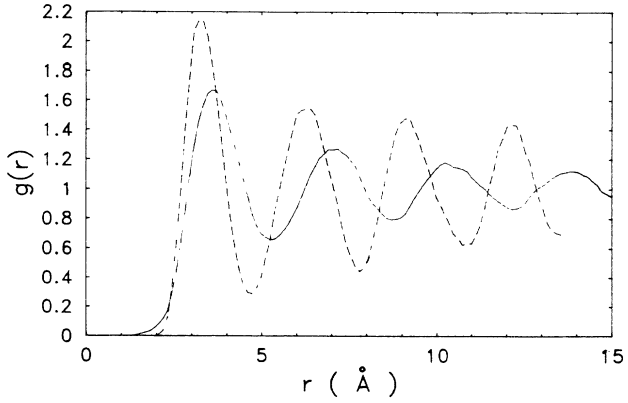

FIG. 5. The radial distribution function for two densities in the triangular solid. The solid line is a density near melting, $\rho=0.0765$ Å^{-2}, and the dashed line is a higher density solid, $\rho=0.0995$ Å^{-2}.

TABLE VIII. Moments of the single-particle distribution function.

Density (Å^{-2})	$\langle r^2 \rangle$	$\langle r^4 \rangle$	β	L
0.0689	0.178±0.007	$(6.3\pm0.5)\times10^{-02}$	$(0.4\pm4.7)\times10^{-04}$	0.264±0.001
0.0765	0.132±0.004	$(3.5\pm0.2)\times10^{-02}$	$(3.4\pm1.7)\times10^{-04}$	0.239±0.002
0.0842	$(9.7\pm0.4)\times10^{-02}$	$(1.9\pm0.2)\times10^{-02}$	$(-1.1\pm1.4)\times10^{-04}$	0.215±0.001
0.0995	$(5.9\pm0.2)\times10^{-02}$	$(6.9\pm0.5)\times10^{-03}$	$(-3.5\pm3.3)\times10^{-05}$	0.182±0.001

um density (see Table IX), the variational value for n_0 is 0.44±0.05 and the GFMC result is 0.36±0.05 for the 64-particle system. Similar values were observed in the 100 particle system, with $n_0^{\rm var}=0.46\pm0.01$ and $n_0^{\rm GFMC}=0.34\pm0.02$. As the density increases, the GFMC result drops rapidly to a value near zero at the freezing density. While the variational value of n_0 drops somewhat with increasing density, the condensate fraction is still substantial at $\rho=0.0658$ Å^{-2}. An important observation needs to be stressed here. At this high density, the GFMC liquid has not yet frozen but the variational liquid is well into the density regime of the variational solid (see Table VII). The simple Jastrow form for the trial function is not a good representation for the high-density liquid. This is seen in the equation of state and is clearly manifested in the calculation of the condensate fraction. The condensate fraction at high densities for the variational wave function differ so much from the mixed estimates that extrapolation is no longer likely to be reliable. A clear picture of the behavior of the high-density liquid awaits the use of the improved variational wave function referred to previously.

The Fourier transform of the one-body density matrix is the momentum distribution $n(k)$. Displayed in Fig. 6 is the momentum distribution near the equilibrium density $\rho=0.0421$ Å^{-2}. The solid line is a sphericalized $n(k)$ obtained by Fourier transforming $n(r)$. The circles with error bars are $n(k)$ calculated directly from the particle configurations at individual wave vectors and all values with $|\mathbf{k}|$ the same have been averaged together. The structure at large k is probably an artifact of the Fourier transform arising from the significant noise in the calculation of $n(r)$.

V. COMPARISONS WITH THREE-DIMENSIONAL ^{4}He AND TWO-DIMENSIONAL CLASSICAL SYSTEMS

A. Three-dimensional ^{4}He

We have results for two quantum-mechanical systems, two-dimensional ^{4}He, and three-dimensional ^{4}He, using the same interaction potential. The difference, of course, is dimensionality. In this section we comment on the differences in the ground-state properties of these two systems. To compare densities, we use reduced densities defined in terms of the characteristic length of the HFDHE2 interaction, $\sigma_{\rm HF}=2.6385$ Å, that distance at which the potential is zero.

Two-dimensional (2D) and three-dimensional (3D) ^{4}He form low-density liquids at zero pressure in the ground state. The striking difference between them is the much lower reduced density, $\rho_0=0.304\sigma_{\rm HF}^{-2}$, of the 2D liquid as compared with the 3D liquid, $\rho_0=0.400\sigma_{\rm HF}^{-3}$. This difference is further emphasized by comparing the mean particle separation,[21] 2.70 and 2.22 Å, respectively. The particles are 22% further apart in 2D than in 3D. Such a difference suggests that there will be rather different binding energies in the two systems. In 2D, the binding energy at zero pressure is 0.84 K/particle, which is much less than the 7.12 K/particle in 3D. Further insight is gained from comparing the balance of kinetic energy $\langle T \rangle$ and potential energy $\langle V \rangle$ in the two systems. The values of $\langle T \rangle$ and potential energy $\langle V \rangle$ are only 18% apart in 2D. In 3D, they are 33% apart.[22]

The larger interparticle distances in the zero pressure 2D system can be expected to affect the correlation functions. The height of the first peak of the radial distribution function near equilibrium is 1.23, 11% lower in 2D than the value in 3D, viz. 1.38. The second peak heights are 1.06 and 1.04, respectively. Turning to the structure function, we find only a 4% difference in the height of the

TABLE IX. Fraction of particles condensed in the zero momentum state from variational and GFMC calculations.

Density (Å^{-2})	$n_0^{\rm var}$	$n_0^{\rm mixed}$	$n_0^{\rm GFMC}$
0.0421	0.44±0.05	0.40±0.01	0.36±0.05
0.0536	0.33±0.02	0.28±0.02	0.24±0.03
0.0612	0.23±0.01	0.15±0.01	0.07±0.02
0.0658	0.25±0.03	0.10±0.01	

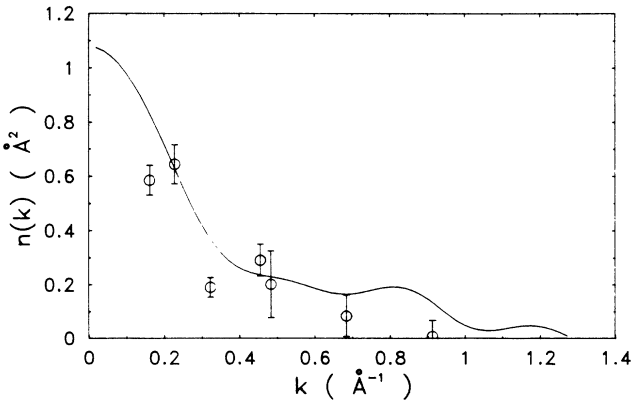

FIG. 6. The momentum distribution in the liquid near equilibrium, $\rho=0.0421$ Å^{-2}. The solid line is the Fourier transform of $n(r)$. The circles with error bars are calculated directly from the particle configurations.

first peak, 1.30 in 2D, and 1.35 in 3D. This similarity is a consequence of the weak spatial correlations shown by both fluids at large distances.

The low reduced density and large mean particle separation of the zero pressure liquid has a great influence on the condensate fraction in the 2D system. The value of n_0 is 36% near the equilibrium density. This is to be compared with 9% at ρ_0 in 3D.

The next striking difference between the two systems is the much wider range of densities over which the 2D system is a liquid than the 3D system. Two-dimensional ^{4}He must be compressed by 60% before freezing takes place at a reduced density, $\rho=0.472\sigma_{\rm HF}^{-2}$. The mean particle separation has been reduced to 2.17 Å. In 3D, freezing takes place after only a 20% compression from the zero pressure density, $\rho=0.481\sigma_{\rm HF}^{-3}$ and the mean particle separation is 2.09 Å. The reduced freezing densities differ by 2% and the particles are only 4% further apart at freezing in the 2D system than in the 3D system. Thus, we conjecture that the very wide range of fluid densities in 2D comes about because the low density zero pressure phase must be compressed to a similar mean particle separation as that at which the 3D fluid ^{4}He freezes. However, the balance of kinetic and potential energy remains quite different in the two systems. In 2D, $\langle T\rangle$ and $\langle V\rangle$ are equal at freezing, while in 3D, they are 24% apart. The 3D system is again more tightly bound at the freezing density.

Since the mean interparticle spacings are similar in the two systems at freezing, it is not surprising that the peak height of the first peak of the radial distribution function is the same value, 1.54, in both systems. The second peak heights are similar as well, 1.13 in 2D and 1.09 in 3D. An indication that there might be somewhat more correlation in the 2D system at freezing is that the first peak of the structure function is 1.69 as compared with a value of 1.6 in 3D.

Based on our previous discussion of the Bose condensate fraction, we would expect that the 2D system at freezing would have a similar value to the 3D system. Unfortunately, our extrapolation procedures break down before we reach the freezing density in 2D, and we are unable to extract the exact value. The 3D fluid has a small condensate fraction of 4% at the freezing density. It is unclear now what value the 2D system will have at freezing.

The melting and freezing transition shows some differences in the two systems. In 3D there is a density difference between the fluid and solid phase of approximately 11%. In 2D the density difference is only 6%. One is tempted to say that the transition is weakly first order. Later we will compare this density difference with the behavior of classical systems. We need to explore the consequences of this speculation with more detailed simulations.

The two-dimensional system forms a triangular solid with a Gaussian distribution of particles about their lattice. The three-dimensional solid was studied in an fcc lattice where the distribution of particles about the lattice sites was nearly Gaussian. The 2D solid melts at a reduced density of $0.501\sigma_{\rm HF}^{-2}$ which corresponds to a nearest-neighbor distance of 4.00 Å. The melting reduced density in 2D is 8% less than the melting reduced density in 3D, $0.540\sigma_{\rm HF}^{-3}$ and the nearest-neighbor distance is 9% smaller in 3D, 3.64 Å. The Lindemann ratio in the 2D system at freezing is 0.25, to be compared with a value of 0.27 in 3D (for a Lennard-Jones system). The height of the first peak of $g(r)$ is somewhat higher in the 2D system, 1.67, than in the 3D system, 1.60. The two solids melt at similar reduced densities; however, the two-dimensional system appears to have greater spatial correlations.

B. Two-dimensional classical systems

It is worthwhile making a few comparisons with simple classical systems. To make these comparisons precise we compare our quantum systems with the classical hard-disc and hard-sphere systems.

Our first comment concerns the freezing densities. When we compare the density differences between the fluid and solid phases, we find a great similarity. In 2D, both quantum and classical systems show about a 5% difference, while in 3D the difference is about 10%. Clearly the 2D transitions are comparatively weak. However, we must point out that both near freezing and in the solid phase 2D and 3D classical systems show much larger spatial correlations. For example, at freezing the height of the first peak of the radial distribution function is about 6 (Ref. 23) in 2D and about 5 (Ref. 24) in 3D. These are strikingly different values from those of the quantum counterparts.

VI. CONCLUSIONS

Our simulation studies provide the following picture of two-dimensional fluid and solid ^{4}He. The fluid forms at zero pressure as a low density and weakly correlated phase. As a consequence, there is a large Bose condensate of 36%. However, the fluid freezes at a similar reduced density as three-dimensional liquid ^{4}He. Many properties of the two-dimensional system near freezing and melting are very similar to those of the three-dimensional system. The melting, freezing transition is probably weakly first order showing only a 6% difference in the densities of the two phases.

We have a major mystery to resolve. At high fluid densities, the configurations from the variational wave function are in some subtle way very different from those generated by the GFMC code. This is revealed in the very different values we have obtained for the condensate function from our variational calculation as compared with the result from the GFMC code, Table IX. We need to investigate the discrepancy in detail. It is an indicator that we need a much improved variational wave function. The new symmetric, translationally invariant wave function that has recently been proposed[18] for three-dimensional ^{4}He may yield interesting new results for the two-dimensional system.

Our next priority will be to implement a code for this new wave function in 2D. With it we will investigate the nature of the freezing transition. Classically in two-

dimensions, it is possible to form a well-ordered solid from a highly disordered state.[25] In other words, one can anneal out the disorder very rapidly. This is thought to be strong evidence that the freezing transition is weakly first order. It will be important to see if the same phenomenon occurs in the quantum system. The new wave function should also allow us to study whether there are topological defects in the solid phase and whether there is diffusion in that phase.

Finally, we plan to embark on simulations of thin films of helium on a substrate. A variational calculation will be undertaken for the surface plus film system using the HFDHE2 potential in which some account will be taken of adsorption-induced effects. Once good trial functions have been identified, Green's-function Monte Carlo simulations can be carried out.

ACKNOWLEDGMENTS

Much of the computations described in this work were performed with the skillful assistance of Vicki Tom. We would like to thank Kevin Schmidt, Joseph Carlson, and L. Bruch for their helpful suggestions. This work was supported by the National Science Foundation under Grant No. DMR-8419083 and by the Applied Mathematical subprogram of the Office of Energy Research, U. S. Department of Energy under Contract No. DE-AC02-76ER03077. Some of the variational calculations were carried out at Boeing Computer Services under a grant of computer time from NSF. All subsequent calculations have been performed on the CRAY's available at the National Center for Supercomputing Applications (NCSA) located at the University of Illinois through a grant of computer time from the NSF.

[1]Farid F. Abraham, Adv. Phys. **35**, 1 (1986).
[2]R. E. Peierls, Ann. Inst. Henri Poincaré **5**, 177 (1935).
[3]N. D. Mermin, Phys. Rev. **176**, 250 (1968).
[4]J. M. Kosterlitz and D. J. Thouless, J. Phys. C **6**, 1181 (1973).
[5]A. D. Novaco, Phys. Rev. A **7**, 678 (1973).
[6]A. D. Novaco, Phys. Rev. A **8**, 3065 (1973).
[7]M. D. Miller, C.-W. Woo, and C. E. Campbell, Phys. Rev. A **6**, 1942 (1972).
[8]C. E. Campbell and M. Schick, Phys. Rev. A **3**, 691 (1971).
[9]T. C. Padmore, Phys. Rev. Lett. **15**, 828 (1974).
[10]K. S. Liu, M. H. Kalos, and G. V. Chester, Phys. Rev. B **13**, 1971 (1976).
[11]X.-Z. Ni and L. W. Bruch, Phys. Rev. B **33**, 4584 (1986).
[12]R. A. Aziz, V. P. S. Nain, J. S. Carley, W. L. Taylor, and G. T. McConville, J. Chem. Phys. **70**, 4330 (1979).
[13]N. Metropolis, A. W. Rosenbluth, M. N. Rosenbluth, A. H. Teller, and E. Teller, J. Chem. Phys. **21**, 1087 (1953).
[14]D. M. Ceperley and M. H. Kalos, in *Monte Carlo Methods in Statistical Physics,* Vol. 7 of *Topics in Current Physics,* edited by K. Binder (Springer, New York, 1979), Chap. 4.
[15]K. E. Schmidt and M. H. Kalos, in *Applications of the Monte Carlo Method in Statistical Physics,* Vol. 36 of *Topics in Current Physics,* edited by K. Binder (Springer, New York, 1984).
[16]K. E. Schmidt and J. W. Moskowitz, J. Stat. Phys. **43**, 1027 (1986).
[17]M. H. Kalos, M. A. Lee, P. A. Whitlock, and G. V. Chester, Phys. Rev. B **24**, 115 (1981).
[18]S. Vitiello, K. Runge, and M. H. Kalos, Phys. Rev. Lett. **60**, 1970 (1988).
[19]P. A. Whitlock, D. M. Ceperley, G. V. Chester, and M. H. Kalos, Phys. Rev. B **19**, 5598 (1979).
[20]Karl Runge (private communication).
[21]The mean particle separation in the liquid was derived from $r^2=\rho/\pi$ in two dimensions and $r^3=3\rho/4\pi$ in three dimensions.
[22]P. A. Whitlock and R. M. Panoff, Can. J. Phys. **65**, 1409 (1987).
[23]John Zollweg (private communication).
[24]J. P. Hansen and I. R. McDonald, *Theory of Simple Liquids* (Academic, New York, 1976), Chap. 4.
[25]Y. Joanna Wong and G. V. Chester, Phys. Rev. B **35**, 3506 (1987).